Ethanol causes cell death and neuronal differentiation defect during initial neurogenesis of the neural retina by disrupting calcium signaling in human retinal organoids

Yu Gong
University-Town Hospital of Chongqing Medical University
Lingling Ge
Third Military Medical University Southwest Hospital
Qiyou Li
Third Military Medical University Southwest Hospital
Jing Gong
Chongqing University College of Bioengineering
Min Chen
Third Military Medical University Southwest Hospital
Hui Gao
Third Military Medical University Southwest Hospital
Jiahui Kang
Third Military Medical University Southwest Hospital
Ting Yu
Chinese People's Liberation Army: People's Liberation Army
Jiawen Li
University-Town Hospital of Chongqing Medical University
Haiwei Xu (haiweixu2001@163.com)
Third Military Medical University Southwest Hospital https://orcid.org/0000-0002-8840-7918

Research Article

Keywords: fetal alcohol syndrome, retinal neurogenesis, ethanol, human retinal organoids, cell death, neuron differentiation; calcium signaling pathway

Posted Date: May 8th, 2023

DOI: https://doi.org/10.21203/rs.3.rs-2730375/v1

Abstract

Background: Over 90% of children with fetal alcohol syndrome live with ocular aberration due to the susceptible and intricate human eye development process. Initial neurogenesis of the neural retina around six-week gestation is the critical period of human eye development while sustaining the highest risk of prenatal ethanol exposure because of ignorance of early pregnancy. However, the influence and mechanism of short-term ethanol exposure on this developmental process of the human neural retina remain largely unknown.

Methods: To faithfully recapitulate the initial retinal neurogenesis of human neural retina, human embryonic stem cell derived retinal organoids (hROs) were induced and identified by immunostaining. Morphological measurement was performed to primarily assess the influence of short-term ethanol exposure on the growth of neural retina. TUNNEL assay, immunostaining, and flow cytometry were utilized to detect cell death, retinal ganglion cell differentiation, and cell cycle progression in hROs. Bulk RNA-seq analysis and cnet plotting were performed to screen signaling pathway and regulated genes of ethanol treatment. GCaMP5G-expressing human embryonic stem cells were constructed by transduction of pLOV-CMV-GCaMP5G and fluorescence-activated cell sorting. Two-photon microscope live calcium imaging were utilized to reveal altered calcium signaling dynamics after ethanol treatment. Quantitative RT-PCR was performed to verify the expression of screened potential targeted genes of ethanol treatment.

Results: The hROs from D24 to D30 well recapitulate the initial neurogenesis of the human neural retina around six-week gestation *in vivo* at the histological, cellular, and molecular level. 1% (v/v) ethanol slowed the growth of hROs by inducing robust cell death and retinal ganglion cell differentiation defect. Calcium signaling dynamics was proved significantly altered and derived from ethanol-induced down-regulation of *RYR1*and *CACNA1S*. Moreover, the calcium-binding protein *RET*, one of the downstream effector genes of the calcium signaling pathway, synergistically integrates ethanol and calcium signals to abort neuron differentiation and cause cell death.

Conclusion: Our study demonstrated that short-term ethanol exposure greatly impaired the initial neurogenesis of hROs by disrupting the *RYR1* related calcium signaling. These results may help us elaborate on more detailed principles of ethanol-induced teratogenesis and instruct the rational application of alcohol and ethanol-contained drugs during pregnancy.

Introduction

Prenatal alcohol exposure results in a set of severe heterogeneous neurodevelopmental conditions termed fetal alcohol syndrome (FAS), characterized by growth retardation, craniofacial anomalies, and neurodevelopmental disruption [1]. FAS is the commonest non-inherited cause of neurological deficit, with a high prevalence rate of up to 55.42 per 1,000 worldwide [2]. Eye is the most sensitive organ for teratogen, and ocular abnormalities occur in over 90% of children with FAS, including coloboma, microphthalmia, and optic nerve hypoplasia [3]. Initial neurogenesis of the embryonic retina around six-

week gestation is the most critical period of human eye development but sustains the highest risk of prenatal ethanol (EtOH) exposure because of ignorance of early pregnancy [4]. Therefore, it calls for a more profound elaboration of the mechanisms of ethanol on the initial neurogenesis of the human embryonic retina.

Retinal neurogenesis is a complex process that involves the formation of the neural retina in the inner wall of the optic cup and the differentiation of multiple retinal neurons in certain spatial and temporal dimensions to develop into a specific intricate neural circuit. As retinal neurogenesis initiates, retinal progenitor cells at the apical of NR start to differentiate into postmitotic differentiating cells with the earliest-born retinal ganglion cell (RGC), then locate at the inner basal layer of the neural retina [5]. The human retina developmental process cannot be recapitulated in vitro until a novel established retinal organoid system based on human embryonic/pluripotent stem cells in recent years. hROs are three-dimensional self-organized aggregates that resemble human retinas at multiple dimensions from the generation of retinal ganglion cells to functional maturation of the retinal neural circuit [6]. Large numbers of publications demonstrate that hROs are reliable models in vitro to investigate the development, disease, toxicology, and drug screening of human retinas [7]. Thus, hROs enable direct exploring the prenatal alcohol exposure on early neurogenesis of human embryonic retinas instead of nonhuman animal retinas [8].

Early neurogenesis is also a matter of calcium [9]. Calcium signals are instrumental for differentiating neural progenitor cells into neurons during nervous system development. Increasing evidence demonstrates that intracellular Ca^{2+} dynamics are necessary and sufficient to initiate the proneural gene expression, cell cycle progression, and neuron axonal maturation [10]. On the other hand, calcium signaling also responds to intrauterine stress, such as valproic acid [11], cholinomimetic agents [12], and virus infection [13], and contributes to neurodevelopmental defects. Moreover, as organized by the Ca^{2+} channel on the cell membrane and endoplasmic reticulum, dynamic Ca^{2+} is restricted in seconds and serves as a more sensitive tool to orchestrate the early neurogenesis both in the physiology and pathological conditions [14], compared with classic secreted signaling molecules such as Shh, Wnts, BMPs, FGFs, and retinoic acid, which are involved in previous FAS related nonhuman animal model [15, 16]. However, the impact of prenatal ethanol exposure on calcium signaling during initial neurogenesis of the human neural retina and the role of calcium signaling in the ethanol-induced human ocular phenotype remain elusive.

In this work, we utilized human retinal organoids (hROs) to decipher the impact and mechanism of ethanol exposure on the initial neurogenesis of human neural retina. We highlighted the role of calcium signaling pathway in the ethanol-induced cell death and neuronal differentiation defect. Moreover, we demonstrated that calcium dynamic alteration in ethanol-treated hROs was attributed to down-regulation of Ryanodine Receptor 1 (*RYR1*) and Calcium Voltage-Gated Channel Subunit Alpha1 S(*CACNA1S*), and transduced by downstream effector *RET* to abort neuron differentiation and cause cell death via MAPK pathway.

Results

Human embryonic stem cells derived retinal organoids faithfully recapitulate the initial neurogenesis of the human neural retina

As the high consistency of early development between hROs and corresponding human fetal retina *in vivo* [17], to recapitulate the initial neurogenesis of human embryonic neural retina around six-week gestation, we determined to explore hROs from D24 to D30 when retinal ganglion cells were just born using a neural retina enriched induction protocol previously provided by Kuwahara et al [18]. Embryonic bodies acquired Rax^+ optic vesicle with unlaminated epithelium morphology at D20 (Fig. 1A, B) and further developed into $SOX2^+CHX10^+$ neural retina at D24 (Fig. 1C). The hROs at D24 contain a large number of $Math5^+$ retinal progenitor cells and differentiating $p27kip1^+$ postmitotic cells at the basal layer of the neural retina (Fig. 1D, E). $Pax6^{+\,strong}$ retinal ganglion precursor cells first emerged at $Sox2^-$ basal layer, accompanying the primitive lamination of neural retina at D24 (Fig. 1F). Retinal ganglion precursor cells continuously differentiated into $Islet1^+Tuj1^+$ immature RGCs at D30 (Fig. 1G). The immature RGCs turned to a mature phenotype with extending outward Tuj1 + axonal processes after hROs were attached to the gelatin-coated plate (Fig. 1H, I). To detect the molecular dynamic of the initial neurogenesis of neural retina in hROs, we constructed a human embryonic stem cell line expressing GCaMP5G, a genetically encoded calcium indicator suit for neural activity imaging [19], with pLOV-CMV-GCaMP5G transfection. More than 90% of cells expressed GCaMP5G indicating differential cellular calcium dynamic in human embryonic stem cell clones and sustained standard cell morphology and pluripotency after flow cytometry sorting (Additional fle 1:Fig.S1; Additional fle 3:Video1). After induction for 24 days, we again harvested hROs with GCaMP5G expressed in the neural retina (Fig. 1J). Retinal progenitor cells at the outer neuroblast layer were clearly labeled with GCaMP5G (Fig. 1K) and exhibited spontaneous robust global calcium transients which are representative of initial neurogenesis of neural retina [9] (Fig. 1L). These data supported that hROs from D24 to D30 well recapitulate the initial neurogenesis of the human neural retina around six-week gestation *in vivo* at the histological, cellular, and molecular level, distinguishing our work from previous model animal research.

Ethanol exposure slows the growth of the neural retina in hROs

Ethanol, a well-known teratogen for human embryonic development, has a role as an antiseptic drug, a polar solvent, a central nervous system depressant, and a disinfectant. Prenatal alcohol exposure during the initial neurogenesis of the neural retina is catastrophic for eye development. To address the impact of ethanol on the initial neurogenesis of the human neural retina, we first assessed the morphological change of hROs after ethanol exposure. The hROs were stochastically divided into four groups which treated ethanol from D24 to D30 with 0% (control, v/v), 1%, 2%, and 3% EtOH, respectively. As hROs continuously grow in the control condition, 3% EtOH directly brought hROs to a dehydrated-like morphology. Treatment with 2% EtOH induced hROs an atrophic phenotype, whereas 1% EtOH almost aborted the growth of neural retinal in hROs (Fig. 2A). The thickness of neural retina at D24 stayed at

about 185 ± 23μm (mean ± SD), grew to 249 ± 24μm during the development. Treatment of 1% EtOH resulted in a suspension of thickness at 187 ± 26μm. In comparison, 2% EtOH resulted in a shrinkage of thickness at 142 ± 40μm (Fig. 2B). Calculation of variance of neural retina thickness also reflected a significant reduction of growth with 1% EtOH and a negative with 2% EtOH (Fig. 2D). In line with this, measurement of the maximum sectional area of hROs and its variance between D30 and D24 also indicated a similar trend that hROs slowly ceased to grow with 1% EtOH and atrophied with 2% EtOH (Fig. 2C, E). To find the most significant altered mechanism in the maximum pathophysiological condition of heavy drinking rather than the toxicology of ethanol on the eye development, we selected 1% EtOH as a concentration for further experiment, lower than that previously described in the zebrafish model research [20].

Ethanol exposure causes neuronal differentiation defect and cell death in neural retina of hROs

Previous studies have focused on the role of ethanol exposure on optic vesicle evagination at an far early stage [21] or the maturation of the optic nerve around the late pre-/postnatal stage [22]. As we found that 1%EtOH robustly reduced the growth rate of the neural retina at the initial neurogenesis stage, we sorted out to investigate the generation of retinal ganglion cells (RGCs), the first-born neuron in the neural retina. Compared with the control group, $Pax6^{+\,strong}$ retinal ganglion precursor cells robustly decreased with 1% EtOH (Fig. 3A, B, I). Moreover, radial migration of immature $Tuj1^{+}$ RGCs along the Nestin + scaffold was impaired, leading immature Tuj1 + RGCs failed to correctly locate at the basal layer of the neural retina (Fig. 3C, D). When attached to the gelatin-coated dish for a week, RGCs in the neural retina could extend their axons out of hROs for up to 2.0 mm long with dense spines in the control condition (Fig. 3E, G, K). However, 1% EtOH weakened the ability of axonal extension and spine maturation of RGCs and leads to a reduction in the axon density, axonal length, and spine density after hROs attachment (Fig. 3F, H, J ~ L).

As the cell death and cell cycle disruption accounts for most ethanol induced neurodevelopmental defects in previous animal model research [23]. Hence, we further investigated the cell death of hROs after ethanol treatment. Immunostaining showed the percentage of cleaved-$caspase3^{+}$ cells in ethanol-treated hROs significantly elevated to more than 22.1 ± 7.6% (mean ± SD) compared with 4.9 ± 1.5% in control hROs (Fig. 4A ~ C), indicated a burst of regulated cell death after ethanol treatment. TUNEL assay showed a similar result: ethanol increased the percentage of $TUNEL^{+}$ cells in hROs from 3.3 ± 0.7% to 23.8 ± 7.0% (Fig. 4D ~ F). To detect the cell cycle, we dissociated the hROs and analyzed the cell cycle with flow cytometric analysis. More than 59.6 ± 7.3% of cells stayed at G1 phase in the control condition while increasing to 82.5 ± 4.8% after ethanol treatment. Consistently, cells in S and G2/M phase dropped to 10.3 ± 2.5% and 7.2 ± 2.4% after ethanol treatment compared with the control group staying at 24.4 ± 5.4% and 16.0 ± 1.9%, respectively (Fig. 4G, H). This result indicated ethanol-induced cell-cycle arrest in the G1 phase of cells in hROs, which supports previous results from animal models [24].

Transcriptome profiling reveals the calcium signaling pathway as a candidate mechanism of cell death and neuronal differentiation defect in ethanol-treated hROs

To investigate the possible molecular mechanism beneath the ethanol-induced cell death and neuronal differentiation defect, we applied bulk RNA-seq analysis of both control hROs and ethanol-treated hROs. Bioinformatics analysis showed that there were a total of 434 (173 genes upregulated and 261 downregulated genes) differentially expressed genes (DEGs) between the control and ethanol-treated hROs (Fig. 5A). Cluster heat maps showed DEGs between the control hROs and ethanol-treated hROs (Fig. 5B). Volcano plots presented the distribution of DEGs as gray, red, and green circles (Fig. 5C). Enrichment analysis in the PaGenBase [25] demonstrated that these DEGs of ethanol-treated hROs could be enriched as retina tissue-specific pattern genes. Enrichment analysis in Cell Type Signatures [26] further identified DEGs of ethanol-treated hROs as embryonic neural stem cells of homo sapiens. To interpret these DEGs for specific biological processes, we next conducted the Gene Ontology (GO) annotation analysis. The terms such as chromosome organization, positive regulation of cell death, visual perception, regulation of cell development, regulation of neuron differentiation, regulation of ion transport, eye development, and response to calcium ion were significantly enriched for ethanol-treated hROs based on gene counts and P-value (Fig. 5F). This result aligned with the previous study about chromosome damage in ethanol-related diseases [27], and supported the biological phenomenon shown in Figs. 3 and 4. It is worth noting that ion transport and calcium ion response were also enriched as significant biological process. Kyoto Encyclopedia of Genes and Genomes (KEGG) pathway annotation further distinguished several pathways such as systemic lupus erythematosus, amyotrophic lateral sclerosis, pathways in cancer, shigellosis, toxoplasmosis, circadian rhythm, and calcium signaling pathway (Fig. 5G). The chromosome related pathway and immune system disruption of teratogenic effects of ethanol exposure has been widely discovered, however the calcium signaling alteration induced by ethanol remained unknown. So, how ethanol altered the calcium signal pathway during initial neurogenesis of the human neural retina aroused our interest.

Ethanol exposure alters the dynamic of calcium signaling in hROs

The genetically encoded calcium indicator and two-photon microscope enabled us to capture the living cellular calcium signaling in hROs without chemotoxicity and phototoxicity. As shown, he neural retina of hROs presented multiple spontaneous calcium spiking regions characterized as global and local transients (Fig. 6A, B). These regions spontaneously actively generated calcium transients at 0.55 ± 0.46 events per minute (mean ± SD) in the local transient domain and at 0.46 ± 0.20 events per minute in global transient domain (Fig. 6C, O, R; Additional fle 3:Video 2). Amplitude and duration of the local calcium transient maintained at 8.5 ± 4.8 Z and 4.8 ± 4.3 seconds, respectively (Fig. 6D, M, N). Amplitude and duration of the global calcium transient maintained were at 4.0 ± 3.2 Z and 17.9 ± 15.8 seconds, respectively (Fig. 6E, P, Q). Ethanol exposure produced a profound effect on the number of calcium spiking domains contributed by a robust increase of local calcium transient (Fig. 6F, G, K, L). The spiking frequency of local and global transient reduced to 0.14 ± 0.08 and 0.16 ± 0.10 events per minute

respectively after ethanol exposure (Fig. 6H, O, R; Additional fle 3:Video 3). For local calcium transient, ethanol exposure did not alter the amplitude but prolonged the duration to 16.2 ± 18.2 seconds (Fig. 6M, N). For global calcium transient, ethanol exposure reduced the amplitude to 2.3 ± 1.8 Z but did not alter the duration (Fig. 6P, Q). These data showed ethanol exposure could significantly increase the numbers of local transient domains, lower local calcium transients' frequency, and prolong its duration. Moreover, ethanol exposure significantly lowered global calcium transients' frequency and reduced amplitude. Together, these results supported that ethanol exposure altered the calcium signaling dynamic in hROs and may induce cell death and neuronal differentiation defect during the initial neurogenesis of the neural retina.

Identification of RYR1 and CACNA1S as regulators of calcium ion transport and RET as synergistic effecter in the calcium signaling pathway of ethanol-treated hROs

To uncover the potential molecular mechanism beneath the ethanol-induced calcium signaling alteration, we next performed the gene set enrichment analysis (GSEA) analysis of DEGs in ethanol-treated hROs to screen target genes of the calcium signaling pathway. As shown, genes involved in voltage-gated calcium channel activity were enriched, and the most significantly changed genes, such as *RYR1* and *CACNA1S*, were selected as candidate target genes (Fig. 7B). *RYR1* encodes the ryanodine receptor 1 on the endoplasmic reticulum and acts as a calcium channel to release the calcium into the cytoplasm [28]. *CACNA1S* encodes the α1S subunit of L-type voltage-dependent calcium channel expressed on the plasm membrane to transport extracellular calcium into the cytoplasm [29]. Both gene expressions were verified by qRT-PCR (Fig. 7C) and could help explain the calcium signaling alteration observed with the two-photon microscope. Besides, to investigate the effector gene of a downstream cascade of the calcium signaling pathway, we further performed Cnet plotting of their associated genes in DEGs of ethanol-treated hROs. In the network, calcium transporters, such as *RYR1* and *CACNA1S*, were included, and the *RET* gene was highlighted as the most related target genes with only its degree ≥ 6 (Fig. 7A). RET has four cadherin-like domains binding of calcium ions and participating transduction of downstream effect of calcium signaling via MAPK- and AKT- cascade that plays a role in cell differentiation and survival. To further understand the critical nodes of the *RET*-related pathway in ethanol-treated hROs, we analyzed these DEGs with the STRING online database to predict the functional protein-protein interaction of RET (Additional fle 2:Fig.S2). Among these results, CTNNB1, VEGFA, KIT, and TH were predicted as candidate interactive proteins which has been demonstrated playing a role in the cell death/survival and neuron differentiation. As a member of the calcium signaling pathway, the Cnet plotting showed *RET* simultaneously participated communities, such as eye development, positive regulation of cell death, and regulation of neuron differentiation, and regulation of cell development. To verify this prospective relation, we confirmed mRNA levels of selected genes, such as the specific retinal ganglion cell transcription factor *POU4F2*,the anti-apoptotic gene *BCL-2*, and its transcriptional repressor, the pro-apoptotic gene *BCLAF1*, and *RET*. The result showed that the mRNA level of *RET*, *BCL-2*, and *POU4F2* were downregulated, but *BCLAF1* was upregulated in ethanol-treated hROs (Fig. 7C, D). This result indicated that *RET* acts as a center effector gene of a calcium signaling pathway in ethanol-induced cell death and neuron differentiation in hROs.

Discussion

Ethanol is a teratogen, and the eye is the most sensitive organ to teratogens. As early as 1910, Stockard et al. discovered that prenatal ethanol exposure could cause abnormal eye development of chicks and fish. In 2002, Strömland et al. reviewed the ocular signs of patients with fetal alcohol syndrome, such as microphthalmia and optic nerve hypoplasia, and proposed that the neural retina is the pivotal toxic target tissue of ethanol [30]. It is generally recognized that pregnant women should not drink alcohol during pregnancy. However, due to alcohol addiction and recreational drug abuse, the risk of prenatal ethanol exposure continues to exist. The risk and degree of prenatal ethanol exposure reach the highest when the early pregnancy is not informed (less than six-week gestation) and the neural retina/brain begins to generate neurons [31]. The initial neurogenesis of the neural retina plays a decisive role in the development of the whole eye, but whether and how ethanol affects this critical process is unclear. Most previous studies are based on animal model and set a long ethanol exposure time in experiments (span across the entire gestation). However, animal experiments of different species for the same question even have contradictory results. It prompted us to study the effect of short-term prenatal ethanol exposure on the initial neurogenesis of the human neural retina using the human retinal organoids.

Retinal ganglion cells are the earliest differentiated neurons during retinal neurogenesis, which determine the primary retinal lamination. Its development deficit often leads to irreversible blindness in patients. Previous studies have shown that ethanol can interfere with the formation of optic vesicles before the differentiation of retinal ganglion cells and even neural retina formation [32]. After the differentiation of retinal ganglion cells, ethanol exposure will reduce the number of axons of retinal ganglion cells and the thickness of optic nerve sheath, and affect the electrophysiological function of the retina to varying degrees [33]. Different time windows of ethanol exposure lead to different cell component abnormalities and morphological changes because of cell-selective and tissue-selective responses to ethanol [34]. Our study found that at the very beginning of RGCs differentiation, short-term prenatal ethanol exposure significantly slowed the growth of the neural retina, reduced the number of RGCs, and aborted their radial migration from the apical to the basal side of the neural retina after the asymmetric division of retinal progenitor cells. The nestin^{+} scaffold has not been significantly affected, which suggests that Tuj1^{+} ganglion cell migration ability might be damaged. At the same time, we found that ethanol inhibited the axon growth of retinal ganglion cells, similar to the inhibition effect of ethanol on the axonal growth of brain neurons [35]. Previous animal experimental studies based on zebrafish and chicks have put forward conflicting views on retinal cell death after ethanol exposure [36, 37]. Our results showed that short-term prenatal ethanol exposure caused significant regulated cell death in the neural retina. At the same time, the cell cycle of the neural retina cells was arrested in G1 phase, which is consistent with the previous animal experimental results [24]. In short, short-term prenatal ethanol exposure does have a critical impact on the initial neurogenesis of the neural retina by inducing cell death and neuronal differentiation defect.

It is known that ethanol can interfere with chromosome assembly, signal molecule secretion, and transcription factors expression, thus participating in the occurrence of cancer occurrence, neuronal

degeneration, immune system diseases, and tissue development abnormalities [27]. This study found, for the first time, that the calcium signal of the neural retina was also significantly changed by ethanol exposure, which suggests that the calcium signaling pathway may also be one of the molecular mechanisms of ethanol induced teratogenesis. Calcium signal is a vital intracellular second messenger. Calcium signals can widely participate in many critical cell functions, such as cell proliferation, death, differentiation, and movement in the development of nervous system and served as a common target in neurological disorders and neurogenesis [38]. We found that short-term prenatal ethanol exposure at the initial neurogenesis of the neural retina would lead to a decreased frequency and amplitude of global calcium transients in hROs. Previous studies have suggested that global calcium transients can directly regulate cell proliferation and gene transcription [39], which can explain the neuronal differentiation defects after ethanol-induced calcium dynamic alteration. RNA-seq data and qRT-PCR verification indicated that these calcium dynamic changes might be mediated by the differential expression of the endoplasmic reticulum calcium channel RYR1 and the α1S subunit of the plasma membrane voltage-gated calcium channel CACNA1S protein caused by ethanol exposure. On the other hand, ethanol exposure led to an increase in the number of local calcium transient regions in hROs, a decrease in the frequency of calcium spiking, and an increase in the duration. This characteristic change of calcium dynamic is similar to the over-enhancement of local calcium transients caused by calcium overload in mitochondria associated with apoptosis [40]. Mechanically, it is worth mentioning that *HSPA8*, the most significant up-regulated gene in RNA-seq, can mediate the influx of calcium ions in plant mitochondria [41, 42]. Meanwhile, *HSPA5*, another member of the HSPA family is clearly engaged in physical interactions with animal endoplasmic reticulum $InsP_3R$ and mitochondrial VDAC1 channel to mediate calcium overload to trigger regulated cell death [43, 44]. Hence we speculated that the cell death in hROs caused by ethanol exposure might be related to the mitochondrial calcium overload associated with the up-regulation of *HSPA8* (Fig. 8).

Calcium signal transduction often requires the activation of downstream effector proteins. Through bioinformatics analysis, we screened the *RET* gene as the core target gene of the calcium signaling pathway during ethanol exposure. RET protein contains cadherin-like calcium binding domains, which can directly respond to changes in calcium concentration [45]. In addition, it is known that RET is directly involved in the differentiation and maturation of neurons and can also regulate cell death through downstream MAPK or AKT signaling pathway [46]. The enrichment analysis of the KEGG pathway found that the MAPK signaling and calcium signaling pathway also produced significant differences in hROs after ethanol exposure (Fig. 5G). The qRT-PCR verification showed that the expression of RET gene and the anti-apoptotic gene *BCL2*, the downstream target gene of ERK1/2 in MAPK signal [47], were significantly down-regulated. Its transcription-inhibitory pro-apoptotic gene *BCLAF1* was significantly up-regulated, supporting that RET-regulated cell death was caused by ethanol exposure through the MAPK signal pathway. At the same time, the specific transcription factor *POU4F2* of retinal ganglion cells was also significantly down-regulated (Fig. 7D). These results support that *RET* gene plays a critical synergetic role in ethanol-induced neuron differentiation defect and cell death (Fig. 8).

Conclusions

To sum up, in this work we explained the causes of cell death and neuron differentiation defects caused by short-term ethanol exposure at the initial neurogenesis of the human neural retina from the perspective of the calcium signaling pathway and obtain the results closest to human development *in vivo* using hROs. These results may help us understand the mechanism of optic nerve hypoplasia and microphthalmia in FAS patients. In the future, utilizing organoid assemblies, neural chimeras, and microfluidic chips for a more realistic developmental environment exposure to ethanol with a dynamic moderate physiological concentration, we could elaborate on more detailed principles of ethanol-induced teratogenesis and instruct the rational application of alcohol and ethanol-contained drugs during pregnancy.

Materials and methods

Human embryonic stem cell culture and transduction of pLOV-CMV-GCaMP5G

All experiments were conducted in accordance with the guidelines established by the Ethics Committee of Southwest Hospital, Third Military Medical University (Army Medical University). Briefly, the H1 line of human embryonic stem cells (RRID: CVCL_9771) was cultured with Essential 8TM Medium (Gibco) and Vitronectin (Gibco). The H1 colonies were passaged as cell clumps every 4 days. For lentiviral transduction, the H1 cells were dissociated by TrypLE™ Express (Gibco) and suspended in Essential 8TM medium containing pLOV-CMV-GCaMP5G (OBiO Technology; multiplicity of infection equal to 5), Y27632 (Sigma, 10 μM), and polybrene (10 μg/mL). The cells were then seeded in a Vitronectin-coated plate. Sixteen hours later, the virus supernatant was removed and fresh Essential 8TM medium containing Y27632 was added, with Y27632 being withdrawn the following day. To enrich infected cells, the cell population was subjected to fluorescence-activated cell sorting as described later.

Fluorescence-activated cell sorting (FACS)

FACS was performed as previously described [48]. Briefly, the cells were sorted using MoFlo XDP (Beckman Coulter). GCaMP5G-positive cells were identified by comparison to samples of wild-type hESCs. Data analysis was conducted using FlowJo 10.2 software (Tree Star).

Induction of human retinal organoids (hROs) and administration of ethanol

The induction of hROs was performed in accordance with our previous study [49]. Briefly, hESCs were dissociated and re-aggregated (9,000 cells per well) using low-cell adhesion 96-well plates (Sumitomo Bakelite) in growth factor-free chemically defined medium (gfCDM) which contained 45% Iscove's

modified Dulbecco's medium (IMDM, Gibco), 45% Hams F12 (F12, Gibco), Glutamax, 1% chemically defined lipid concentrate (Gibco), 10% Knockout Serum Replacement (KSR) (Gibco), monothioglycerol (450 μM, Sigma), 100 U/mL penicillin, and 100 μg/mL streptomycin (Gibco). Note the gfCDM was supplemented with 20 μM Y-27632 (Sigma) only for the re-aggreation step. On day 6, the culture medium was replaced with fresh gfCMD supplemented with recombinant human BMP4 (PeproTech) at a final concentration of 1.5 nM. Half of the BPM4 containing gfCMD was changed every 3rd day until the hROs were transferred to ultra-low adhesion 9-cm Petri dishes (Corning) on day 18 for further suspension culture with long-term culture medium (LTCM). LTCM contained DMEM/F12-Glutamax medium (Gibco), 10% fetal bovine serum (FBS), 1% N2 supplement (Gibco), 0.1 mM taurine (Sigma), 0.5 μM retinoic acid (Sigma), 0.25 μg/mL Fungizone (Gibco), 100 U/mL penicillin, and 100 μg/mL streptomycin (Gibco). The hROs with primitive NR on day 24 were collected and ethanol was added to the LTCM during days 24 to 30 at a final concentration of 1% (v/v) and refreshed daily.

Immunofluorescence

Immunofluorescence was performed as we previously described [50]. The hROs were fixed with 4% (wt/vol) phosphate-buffered formaldehyde solution and equilibrated in 30% (wt/vol) sucrose solution at 4°C overnight. The specimens were transferred in liquid optimal cutting temperature compound (Biosharp) and frozen at -80°C. Cryosections were produced using a Leica CM1900UV cryostat with a thickness of 10–14μm. For immunofluorescence, the cryosections were blocked with phosphate buffered saline containing 0.1% (vol/vol) Triton X-100, 10% (vol/vol) fetal bovine serum, and 1% (wt/vol) bovine serum albumin (BSA) for 60 minutes at room temperature. The primary antibodies were incubated overnight at 4°C. The 2nd day, the cryosections were incubated with the secondary antibodies diluted as 1:1000 (Alexa Fluor 488, Invitrogen; Alexa Fluor 594, Invitrogen) for 1–2 hours at room temperature. DAPI (1:10, Beyotime) was applied for 10 minutes to counterstain nuclei, followed by cover-slipping with the antifade mounting medium (Beyotime).The related antibodies are listed as below: Rax (Abcam Cat# ab23340, 1:500), Pax6 (Abcam Cat# ab78545, 1:500), Chx10 (Abcam Cat# ab93715, 1:500), Sox2 (Abcam Cat# ab97959, 1:500), Nestin (Sigma-Aldrich Cat# N5413, 1:200), p27Kip1 (Abcam Cat# ab32034, 1:500); Tuj1 (Cell Signaling Technology Cat# 4466, 1:200), Math5 (Abcam Cat# 229245, 1:500); Islet1 (Abcam Cat# 178400, 1:500); Nanog (Abcam Cat# 109250, 1:500); OCT4 (Abcam Cat# 181557, 1:500); SSEA4 (Santa Cruz, sc-59368, 1:500), and cleaved-caspase3 (Cell Signaling Technology Cat# 9664, 1:500).

Live calcium-imaging recordings of hROs-GCaMP5G using two-photon microscopy

Calcium imaging was performed as previously described [51]. The hROs were incubated in DMEM/F12 without phenol red (Abcam Cat# 11-039-021) at room temperature. A moveable objective microscope (Sutter) equipped with a Chameleon titanium-sapphire laser tuned to 915 nm (Coherent) was used, and an Olympus LUM-PlanFI 40× water immersion objective (NA 0.8) was employed. The emitted

fluorescence was captured by the objective and filtered using an HQ 535/50GFP emission filter (Chroma Technology) before detection using Pho Image v.3.0 software. Images were acquired at 1 ms per line using 256×256 per frame and further analyzed with Igor Pro v.6.10 and ImageJ v.1.53t. The regions of interest were defined by the semi-automatic analysis method described previously [52]. Signal acquisition were transferred as scan-normalized fluorescence (Z score), which was calculated as belowed: $\triangle F/F=(F-F0)/F0$, where F is the instantaneous GCaMP5G fluorescence and F0 is the baseline fluorescence of GCaMP5G.

TUNEL assays

The TdT-mediated dUTP-X nick end labeling (TUNEL) assays were performed using the In Situ Cell Death Detection Kit (Roche, Basel, Switzerland). Buffer 1 and buffer 2 were composed as the reaction mixture at a mixed ratio of 1:9 and then diluted 1:3 with phosphate buffered saline buffer. The hROs cryosections were further incubated with the reaction mixture at 37°C for 30 min. Nuclei were counterstained with DAPI (1:10, Beyotime) for 10 min. The sealed slides were photographed using an LSM880 microscope (Zeiss), and images were analyzed using ImageJ v.1.53t.

Bulk RNA-sequencing profiling and GSEA analysis

Bulk RNA-sequencing was performed as previously described [53] to identify gene profile changes between control and ethanol-treated groups of hROs at D30. RNA was extracted using TRIzol reagent (Gibco) and reverse transcribed using the PrimeScript RT Reagent Kit (Takara, Japan), and then isolated using Oligo (dT)-attached magnetic beads. The cDNA fragments were amplified and constructed using an Agilent 2100 Bioanalyzer (CA) and an ABI StepOnePlus Real-Time PCR System.The qualified cDNA libraries were sequenced by the Illumina HiSeq with a 150-bp paired-end model. The gene expressions were measured using Fragments Per Kilobase of exon per Million fragments mapped (FPKM). Genes with q-value < 0.00001 and fold change > 1.0 were defined as differentially expressed genes (DEGs). Gene Ontology (GO) term enrichment and Kyoto Encyclopedia of Genes and Genomes (KEGG) pathway enrichment were performed on the Metascape platform (metascape.org) to annotate the unique biological processes and enriched pathways of DEGs. GSEA was performed using the GSEA software (http://software.broadinstitute.org/gsea/).

Quantitative Real-time polymerase chain reaction (RT-PCR)

Total RNA was extracted from hROs using TRIzol reagent (Gibco). Reverse-transcription was performed with the PrimeScript® RT Reagent Kit (Takara). The cDNA was amplified with specific gene primers (listed below). Quantitative RT-PCR was performed through the CFX96 Real-Time PCR System (Bio-Rad) with at least three separate RNA hROs samples. RYR1, For CACCAATGGCCTATACAACCAG, Rev GCTCAGGATAACGCCCTCG; CACNA1S, For TTGCCTACGGCTTCTTATTCCA, Rev GTTCCAGAATCACGGTGAAGAC; POU4F2, For CTCGCTCGAAGCCTACTTTG, Rev

GACGCGCACCACGTTTTTC; RET, For GCGATGTTGTGGAGACCCAA, Rev AGCACCGAGACGATGAAGGA; BCL2, For GGTCGCCAGGACCTCGCCGCTG, Rev GGTTGACGCTCTCCACACACAT; BCLAF1, For AGGTCTGGGTCTGGTTCTGTTG, Rev GAAGCCTCTTTATCCCTGGTAT. In this study, three independent experiments were performed.

Quantification of the NR thickness, volume and attached axons

Morphological images of hROs were captured by a Leica DMI3000 microscope. The thickness of the neuroretina (NR) and the maximum diameter were measured using ImageJ v.1.53t, as shown in Fig. 2A. After attaching the hROs to a gelatin-coated dish for an additional week, axons and spines were counted in a clockwise direction using ImageJ.

Microscopy, image acquisition, and processing

The high-resolution acquisition of immunostaining images was achieved with a Zeiss LSM880 confocal microscope. Images were processed by ImageJ v.1.53t and Illustrator CC 2017 (Adobe).

Statistical analysis

Visualized data in figures were presented as means ± SEM and numerical data in text were presented as means ± SD. Statistical tests were performed using PRISM software (GraphPad, version 9.0.0). Two-tailed, unpaired t-tests were used for pairwise comparisons, and one-way ANOVA with Tukey's or Dunnett's correction was used for multiple comparisons. Statistical significance was set at a P-value < 0.05.

Abbreviations

FAS Fetal alcohol syndrome

hROs Human embryonic stem cells derived retinal organoids

EtOH Ethanol

RGC Retinal ganglion cell

RYR1 Ryanodine Receptor 1

CACNA1S Calcium Voltage-Gated Channel Subunit Alpha1

DEGs Differentially expressed genes

GO Gene Ontology

KEGG Kyoto Encyclopedia of Genes and Genomes

GSEA Gene set enrichment analysis

FACS Fluorescence-activated cell sorting

gfCDM Growth factor-free chemically defined medium

IMDM Iscove's modified Dulbecco's medium

KSR Knockout Serum Replacement

LTCM Long-term culture medium

BSA Bovine serum albumin

TUNEL TdT-mediated dUTP-X nick end labeling

FPKM Fragments Per Kilobase of exon per Million fragments mapped

RT-PCR Quantitative Real-time polymerase chain reaction

NR Neuroretina

Declarations

Acknowledgments

We thank Prof. Xiaotang Fan, Dr.Xiangyu He, and Miss. Yajie Fang for their kindly assistance in the early research and revision discussion.

Author contributions

YG, LG, QL, JG, MC, HG, JK, and TY performed the experiments and analyzed the results. JL and HX designed the project and directed the research. YG and LG wrote the manuscript.

Funding

This study was funded by the National Key Research and Development Program of China grants 2021YFA1101203, and the National Natural Science Foundation of China grants 31930068.

Availability of data and materials

The datasets generated during and/or analyzed in the current study are available on reasonable request.

Declarations

Ethics approval and consent to participate

Not applicable.

Consent for publication

All the authors agreed to its publication.

Institutional Review Board Statement

Not applicable.

Competing interests

All authors declare no competing or financial interests.

References

1. Mattson SN, Bernes GA, Doyle LR. Fetal Alcohol Spectrum Disorders: A Review of the Neurobehavioral Deficits Associated With Prenatal Alcohol Exposure. Alcoholism, clinical and experimental research. 2019;43(6):1046–62.
2. Roozen S, Peters GJ, Kok G, Townend D, Nijhuis J, Curfs L. Worldwide Prevalence of Fetal Alcohol Spectrum Disorders: A Systematic Literature Review Including Meta-Analysis. Alcohol Clin Exp Res. 2016;40(1):18–32.
3. Abdelrahman A, Conn R. Eye abnormalities in fetal alcohol syndrome. Ulster Med J. 2009;78(3):164–5.
4. Ethen MK, Ramadhani TA, Scheuerle AE, Canfield MA, Wyszynski DF, Druschel CM, et al. Alcohol consumption by women before and during pregnancy. Matern Child Health J. 2009;13(2):274–85.
5. Centanin L, Wittbrodt J. Retinal neurogenesis. Development. 2014;141(2):241–4.
6. Zhang Z, Xu Z, Yuan F, Jin K, Xiang M. Retinal Organoid Technology: Where Are We Now? Int J Mol Sci. 2021;22:19.
7. Dorgau B, Georgiou M, Chaudhary A, Moya-Molina M, Collin J, Queen R, et al. Human Retinal Organoids Provide a Suitable Tool for Toxicological Investigations: A Comprehensive Validation Using Drugs and Compounds Affecting the Retina. Stem Cells Transl Med. 2022;11(2):159–77.
8. Horejs C. Organ chips, organoids and the animal testing conundrum. Nat Rev Mater. 2021;6(5):372–3.
9. Leclerc C, Néant I, Moreau M. Early neural development in vertebrates is also a matter of calcium. Biochimie. 2011;93(12):2102–11.
10. Toth AB, Shum AK, Prakriya M. Regulation of neurogenesis by calcium signaling. Cell Calcium. 2016;59(2–3):124–34.

11. Kim JW, Oh HA, Kim SR, Ko MJ, Seung H, Lee SH, et al. Epigenetically Upregulated T-Type Calcium Channels Contribute to Abnormal Proliferation of Embryonic Neural Progenitor Cells Exposed to Valproic Acid. Biomol Ther (Seoul). 2020;28(5):389–96.
12. Paladino O, Moranda A, Falugi C. Spatiotemporal role of muscarinic signaling in early chick development: exposure to cholinomimetic agents by a mathematical model.Cell Biol Toxicol. 2022.
13. Sison SL, O'Brien BS, Johnson AJ, Seminary ER, Terhune SS, Ebert AD. Human Cytomegalovirus Disruption of Calcium Signaling in Neural Progenitor Cells and Organoids.J Virol. 2019;93(17).
14. Bootman MD, Bultynck G. Fundamentals of Cellular Calcium Signaling: A Primer.Cold Spring Harbor perspectives in biology. 2020;12(1).
15. Brennan D, Giles S. Sonic hedgehog expression is disrupted following in ovo ethanol exposure during early chick eye development. Reproductive Toxicol (Elmsford NY). 2013;41:49–56.
16. Kahn BM, Corman TS, Lovelace K, Hong M, Krauss RS, Epstein DJ. Prenatal ethanol exposure in mice phenocopies Cdon mutation by impeding Shh function in the etiology of optic nerve hypoplasia. Dis Models Mech. 2017;10(1):29–37.
17. Sridhar A, Hoshino A, Finkbeiner CR, Chitsazan A, Dai L, Haugan AK, et al. Single-Cell Transcriptomic Comparison of Human Fetal Retina, hPSC-Derived Retinal Organoids, and Long-Term Retinal Cultures. Cell Rep. 2020;30(5):1644–59e4.
18. Kuwahara A, Ozone C, Nakano T, Saito K, Eiraku M, Sasai Y. Generation of a ciliary margin-like stem cell niche from self-organizing human retinal tissue. Nat Commun. 2015;6:6286.
19. Akerboom J, Chen TW, Wardill TJ, Tian L, Marvin JS, Mutlu S, et al. Optimization of a GCaMP calcium indicator for neural activity imaging. J Neurosci. 2012;32(40):13819–40.
20. Muralidharan P, Sarmah S, Marrs JA. Zebrafish retinal defects induced by ethanol exposure are rescued by retinoic acid and folic acid supplement. Alcohol. 2015;49(2):149–63.
21. Santos-Ledo A, Cavodeassi F, Carreño H, Aijón J, Arévalo R. Ethanol alters gene expression and cell organization during optic vesicle evagination. Neuroscience. 2013;250:493–506.
22. Pons-Vazquez S, Gallego-Pinazo R, Galbis-Estrada C, Zanon-Moreno V, Garcia-Medina JJ, Vila-Bou V et al. Combined pre- and postnatal ethanol exposure in rats disturbs the myelination of optic axons. Alcohol and alcoholism (Oxford, Oxfordshire). 2011;46(5):514 – 22.
23. Ehrhart F, Roozen S, Verbeek J, Koek G, Kok G, van Kranen H, et al. Review and gap analysis: molecular pathways leading to fetal alcohol spectrum disorders. Mol Psychiatry. 2019;24(1):10–7.
24. Chung HY, Chang CT, Young HW, Hu SP, Tzou WS, Hu CH. Ethanol inhibits retinal and CNS differentiation due to failure of cell cycle exit via an apoptosis-independent pathway. Neurotoxicol Teratol. 2013;38:92–103.
25. Pan JB, Hu SC, Shi D, Cai MC, Li YB, Zou Q, et al. PaGenBase: a pattern gene database for the global and dynamic understanding of gene function. PLoS ONE. 2013;8(12):e80747.
26. Subramanian A, Tamayo P, Mootha VK, Mukherjee S, Ebert BL, Gillette MA, et al. Gene set enrichment analysis: a knowledge-based approach for interpreting genome-wide expression profiles. Proc Natl

Acad Sci U S A. 2005;102(43):15545–50.

27. Hodskinson MR, Bolner A, Sato K, Kamimae-Lanning AN, Rooijers K, Witte M et al. Alcohol-derived DNA crosslinks are repaired by two distinct mechanisms.Nature. 2020.
28. des Georges A, Clarke OB, Zalk R, Yuan Q, Condon KJ, Grassucci RA, et al. Structural Basis for Gating and Activation of RyR1. Cell. 2016;167(1):145–57e17.
29. Schartner V, Romero NB, Donkervoort S, Treves S, Munot P, Pierson TM, et al. Dihydropyridine receptor (DHPR, CACNA1S) congenital myopathy. Acta Neuropathol. 2017;133(4):517–33.
30. Strömland K, Pinazo-Durán MD. Ophthalmic involvement in the fetal alcohol syndrome: clinical and animal model studies. Alcohol Alcohol (Oxf Oxfs). 2002;37(1):2–8.
31. May PA, Gossage JP. Maternal risk factors for fetal alcohol spectrum disorders: not as simple as it might seem. Alcohol Res Health. 2011;34(1):15–26.
32. Kennelly K, Brennan D, Chummun K, Giles S. Histological characterisation of the ethanol-induced microphthalmia phenotype in a chick embryo model system. Reproductive Toxicol (Elmsford NY). 2011;32(2):227–34.
33. Harris SJ, Wilce P, Bedi KS. Exposure of rats to a high but not low dose of ethanol during early postnatal life increases the rate of loss of optic nerve axons and decreases the rate of myelination.J Anat. 2000;197 Pt 3:477 – 85.
34. Santos-Ledo A, Arenzana FJ, Porteros A, Lara J, Velasco A, Aijon J, et al. Cytoarchitectonic and neurochemical differentiation of the visual system in ethanol-induced cyclopic zebrafish larvae. Neurotoxicol Teratol. 2011;33(6):686–97.
35. Zhu Y, Wang L, Yin F, Yu Y, Wang Y, Shepard MJ, et al. Probing impaired neurogenesis in human brain organoids exposed to alcohol. Integr Biol (Camb). 2017;9(12):968–78.
36. Kashyap B, Frederickson LC, Stenkamp DL. Mechanisms for persistent microphthalmia following ethanol exposure during retinal neurogenesis in zebrafish embryos. Vis Neurosci. 2007;24(3):409–21.
37. Tufan AC, Abban G, Akdogan I, Erdogan D, Ozogul C. The effect of in ovo ethanol exposure on retina and optic nerve in a chick embryo model system. Reproductive Toxicol (Elmsford NY). 2007;23(1):75–82.
38. Glaser T, Arnaud Sampaio VF, Lameu C, Ulrich H. Calcium signalling: A common target in neurological disorders and neurogenesis. Semin Cell Dev Biol. 2019;95:25–33.
39. Dupont G, Combettes L, Bird GS, Putney JW. Calcium oscillations.Cold Spring Harbor perspectives in biology. 2011;3(3).
40. Humeau J, Bravo-San Pedro JM, Vitale I, Nuñez L, Villalobos C, Kroemer G, et al. Calcium signaling and cell cycle: Progression or death. Cell Calcium. 2018;70:3–15.
41. Liu SY, Yuan D, Sun RJ, Zhu JJ, Shan NN. Significant reductions in apoptosis-related proteins (HSPA6, HSPA8, ITGB3, YWHAH, and PRDX6) are involved in immune thrombocytopenia. J Thromb Thrombolysis. 2021;51(4):905–14.

42. Fu S, Li L, Kang H, Yang X, Men S, Shen Y. Chronic mitochondrial calcium elevation suppresses leaf senescence. Biochem Biophys Res Commun. 2017;487(3):672–7.
43. Szabadkai G, Bianchi K, Várnai P, De Stefani D, Wieckowski MR, Cavagna D, et al. Chaperone-mediated coupling of endoplasmic reticulum and mitochondrial Ca2 + channels. J Cell Biol. 2006;175(6):901–11.
44. Szalai G, Krishnamurthy R, Hajnóczky G. Apoptosis driven by IP(3)-linked mitochondrial calcium signals. Embo j. 1999;18(22):6349–61.
45. Shabbir A, Kojadinovic A, Shafiq T, Mundi PS. Targeting RET alterations in cancer: Recent progress and future directions.Crit Rev Oncol Hematol. 2022:103882.
46. Regua AT, Najjar M, Lo HW. RET signaling pathway and RET inhibitors in human cancer. Front Oncol. 2022;12:932353.
47. Liu YZ, Boxer LM, Latchman DS. Activation of the Bcl-2 promoter by nerve growth factor is mediated by the p42/p44 MAPK cascade. Nucleic Acids Res. 1999;27(10):2086–90.
48. Liu Y, Carlsson R, Ambjørn M, Hasan M, Badn W, Darabi A, et al. PD-L1 expression by neurons nearby tumors indicates better prognosis in glioblastoma patients. J Neurosci. 2013;33(35):14231–45.
49. Gong Y, He X, Li Q, He J, Bian B, Li Y et al. SCF/SCFR signaling plays an important role in the early morphogenesis and neurogenesis of human embryonic neural retina.Development. 2019;146(20).
50. Li QY, Zou T, Gong Y, Chen SY, Zeng YX, Gao LX, et al. Functional assessment of cryopreserved clinical grade hESC-RPE cells as a qualified cell source for stem cell therapy of retinal degenerative diseases. Exp Eye Res. 2021;202:108305.
51. He XY, Zhao CJ, Xu H, Chen K, Bian BS, Gong Y, et al. Synaptic repair and vision restoration in advanced degenerating eyes by transplantation of retinal progenitor cells. Stem Cell Reports. 2021;16(7):1805–17.
52. Agarwal A, Wu PH, Hughes EG, Fukaya M, Tischfield MA, Langseth AJ, et al. Transient Opening of the Mitochondrial Permeability Transition Pore Induces Microdomain Calcium Transients in Astrocyte Processes. Neuron. 2017;93(3):587–605. e7.
53. Li M, Zeng Y, Ge L, Gong J, Weng C, Yang C, et al. Evaluation of the influences of low dose polybrominated diphenyl ethers exposure on human early retinal development. Environ Int. 2022;163:107187.

Figures

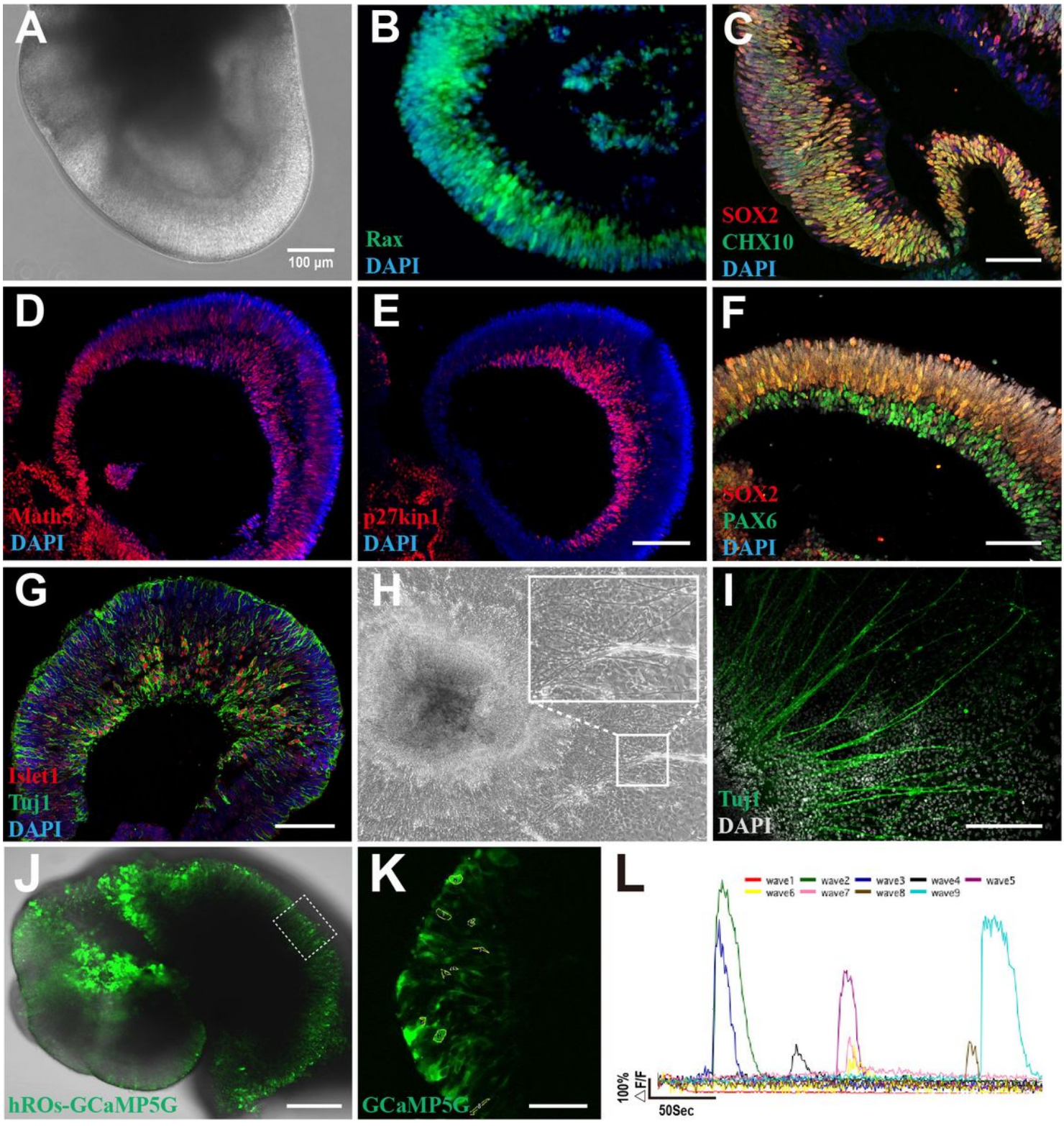

Figure 1

Identification of initial neurogenesis of human neural retina in human embryonic stem cells derived retinal organoids (hROs). **A** Bright field view showing the typical epithelium morphology of hROs at D20 with induction protocol. **B-C** Immunostaining showed hROs with the Rax^{+} optic vesicle at D20 (**B**) and $Sox2^{+}Chx10^{+}$ neural retina at D24 (**C**). **D-E** Cells of hROs at D24 showing neurogenic competence ($Math5^{+}$ **D**) and exit of cell cycle ($p27kip1^{+}$ **E**) to ready to differentiate into neurons. $Pax6^{+strong}$ retinal

ganglion precursor cells (**F)** emerge at the $Sox2^-$ inner basal layer of hROs at D24 and gradually specified into immature $Islet1^+Tuj1^+$ RGC (**G)** at D30. These immature RGC further differentiated into mature neuron which extend $Tuj1^+$ axonal fiber (**I)** after attached on the gelatin-coated dish (**H)**. **J** hROs derived from GCaMP5G-expressing human embryonic stem cells exhibited positive green fluorescent under inverted fluorescence microscope. **K** Two-photon microscopy captured the differential cytosolic GCaMP5G of retinal progenitor cells at the outer neuroblast layer of hROs. The yellow circle indicated regions of interest gated by ImageJ. **L** Time-lapse imaging with two-photon microscopy depicted nine global Ca^{2+} transients of retinal progenitor cells in hROs. Scale bar: 100um, **A~J**; 50um, **K**.

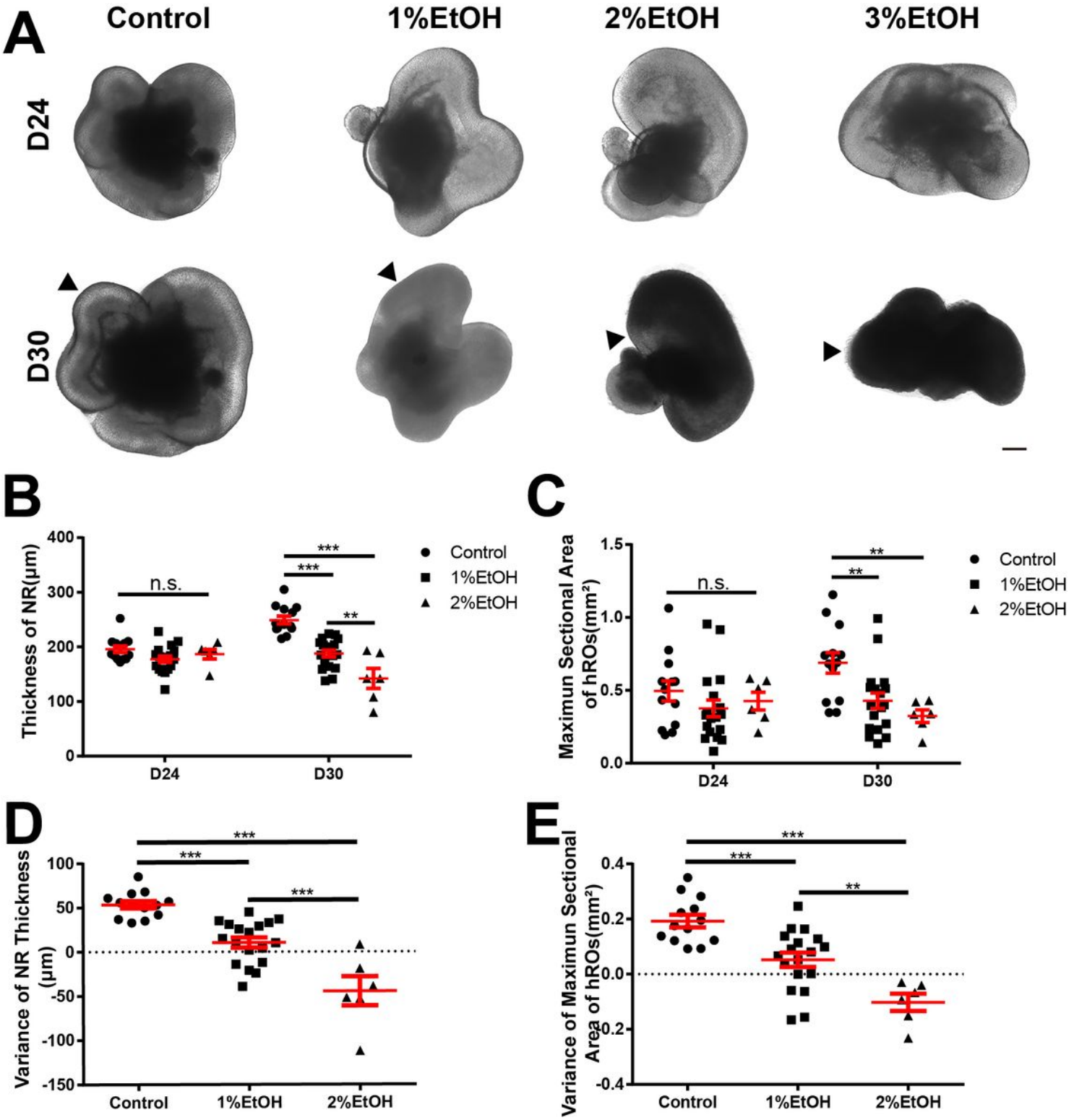

Figure 2

Neural retina in hROs retards its growth after ethanol exposure. **A** Bright field view showing the morphological change during D24~D30 with different ethanol concentration(v/v). Black arrow heads indicate the laminated neural retina (NR) of hROs. 3% ethanol directly induce a necrocytosis phenotype as 2% induce an atrophy phenotype of neural retina of hROs. Only 1% ethanol induce a retardation phenotype. Measurement of NR thickness and maximum sectional area of hROs exposed to 0%, 1%, and

2% ethanol respectively at D24 and D30. Thickness of NR (**B)** and maximum sectional area of hROs (**C)** both decreased in a concentration dependent manner of ethanol. **D-E** Variance of NR thickness and maximum sectional area of hROs from D24 to D30 exposed to 0%, 1%, and 2% ethanol. A significant developmental retardation of hROs was induced by 1% ethanol exposure whilst an atrophy of hROs was induced by 2% ethanol exposure (n=13, 18, and 6 for each group from three independent experiments). Data are presented as mean ± s.e.m. and were collected from three independent experiments. *p < 0.05; **p < 0.01; ***p < 0.005. Scale bars: 200 μm.

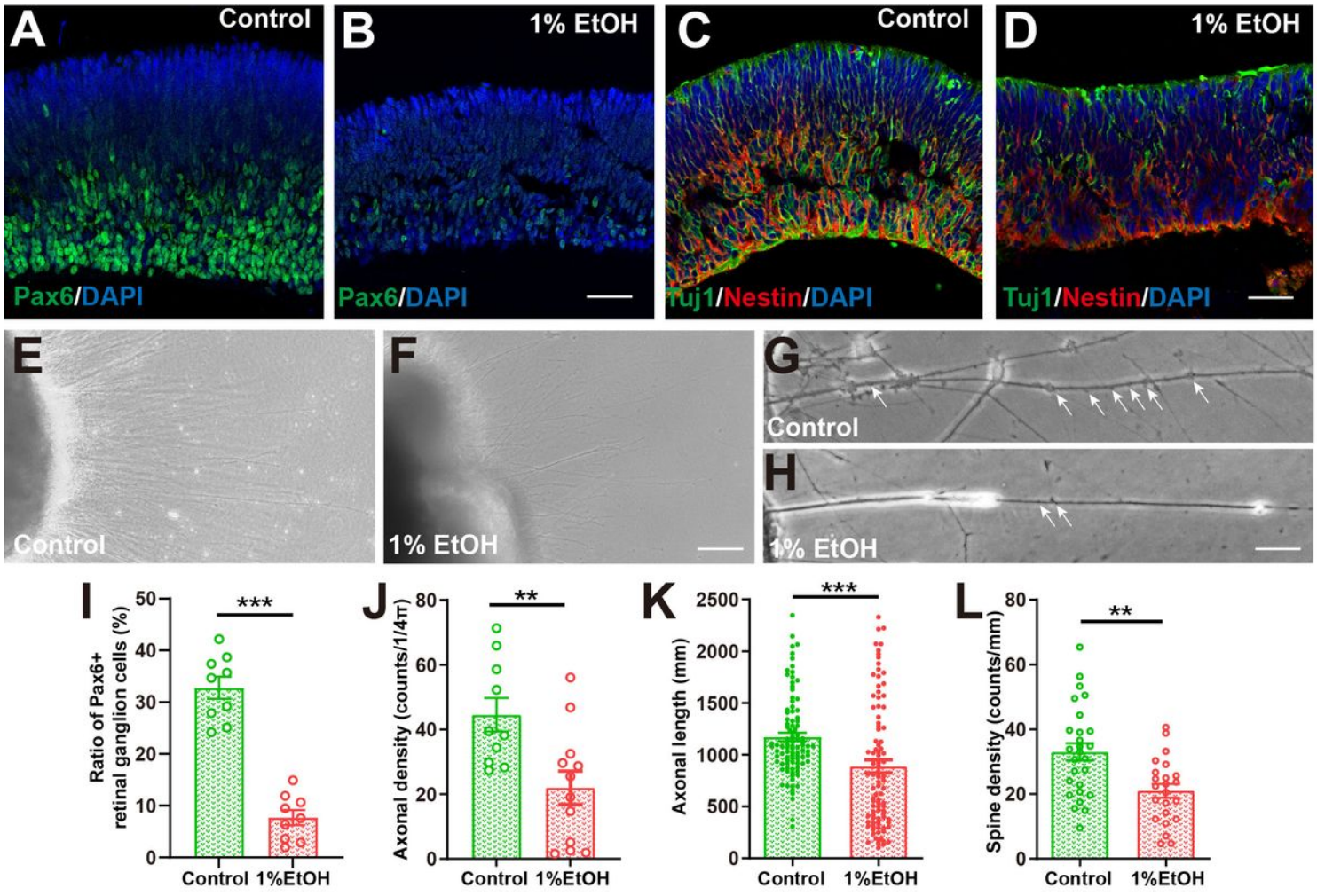

Figure 3

Ethanol impairs the specification, radial migration, and axonal growth of retinal ganglion cells in hROs. Immunostaining showing Pax6$^{+strong}$ retinal ganglion precursor cells mainly distributed at the inner basal layer of hROs (**A**) and robustly decreased after the ethanol treatment at D30 (**B**). Immunostaining showing radial migration of immature Tuj1+ RGC along the nestin+ basal scaffold and located at the inner basal layer of hROs (**C**) whilst it failed to migrate and as a result dislocated at the apical side of neural retina in ethanol-treated hROs (**D**). Representatives of the hROs attached to the gelatin-coated dish for a week (Control for **E**, Ethanol for **F**) and magnified bright field view of the axon and spine (Control for **G**, 1% EtOH for **H**), white arrow indicates the spine along the extended axon. Quantification of the Pax6+ retinal ganglion precursor cells (**I,** n=9 and 9), axonal density (**J,** n=10 and 12), axonal length (**K,** n=95 and

95) of attached hROs, and spine density of axon (**L,** n=27 and 23). Data are presented as mean ± s.e.m. and were collected from three independent experiments. *p < 0.05; **p < 0.01; ***p < 0.005. Scale bars: 50 μm for **A~F**; 5μm for **G** and **H**.

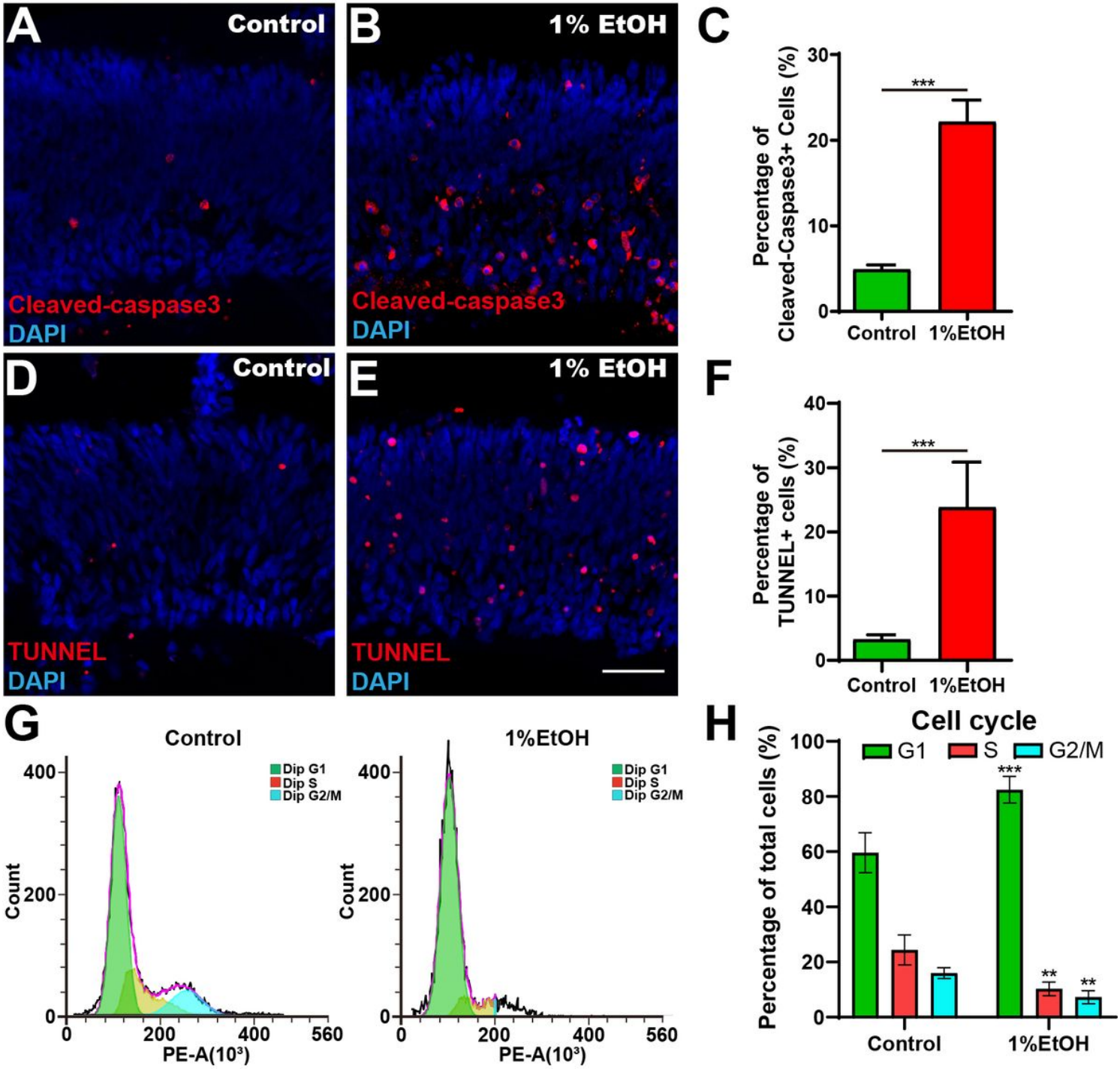

Figure 4

Ethanol causes cell death and cell cycle arrest in hROs. **A** Representatives of cleaved-caspase3^{+} apoptotic cells in D30 hROs without ethanol treatment**. B** Representatives of cleaved-caspase3^{+} apoptotic cells in D30 hROs treated with 1% EtOH from D24~D30. **C** Quantification of cleaved-caspase3^{+} apoptotic cells in D30 hROs both in control and ethanol group (n=9 and 9 for each group). **D** Representatives of

TUNEL assay staining in D30 hROs without ethanol treatment**. E** Representatives of TUNEL assay staining in D30 hROs treated with 1% EtOH from D24~D30. **F** Quantification of TUNEL assay staining in D30 hROs both in control and ethanol group (n=9 and 9 for each group). **G** Cell cycle analysis by flow cytometry showed cell-cycle arrest in G1 phase in ethanol treated hROs. **H** Quantification of cell cycle component in D30 hROs both in control and ethanol group (n=3 independent experiments). Data are presented as mean ± s.e.m. and were collected from three independent experiments. *p < 0.05; **p < 0.01; ***p < 0.005. Scale bars: 50 μm for **A~E.**

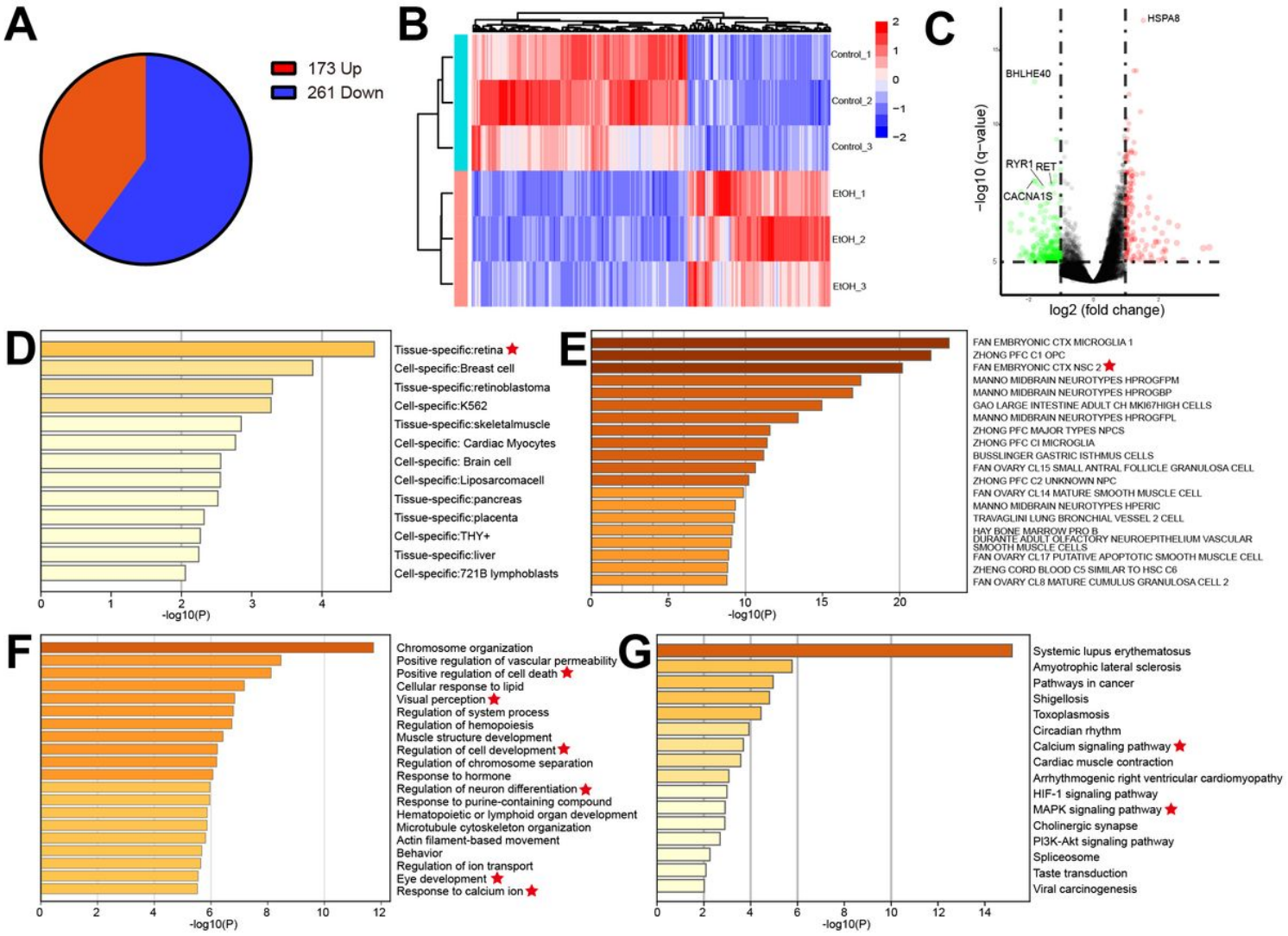

Figure 5

The RNA-Seq analysis of control hROs and ethanol-treated hROs at D30. **A** The number of differentially expressed genes (DEGs) in hROs after treatment with 1% EtOH for D24~D30. **B** Cluster heatmap of hROs between control and ethanol-treated hROs (n=3, three independent experiments). **C** Volcano plot displaying significant DEGs in hROs after treatment with 1% EtOH for D24~D30. **D** Summary of enrichment analysis in PaGenBase. **E** Summary of enrichment analysis in Cell Type Signatures. **F** Top 20 of GO annotation for biological processes of DEGs in hROs after treatment with 1% EtOH for D24~D30. **G**

Top 16 of KEGG enrichment pathway of DEGs in hROs after treatment with 1% EtOH for D24~D30. Red asterisk represents items of interest.

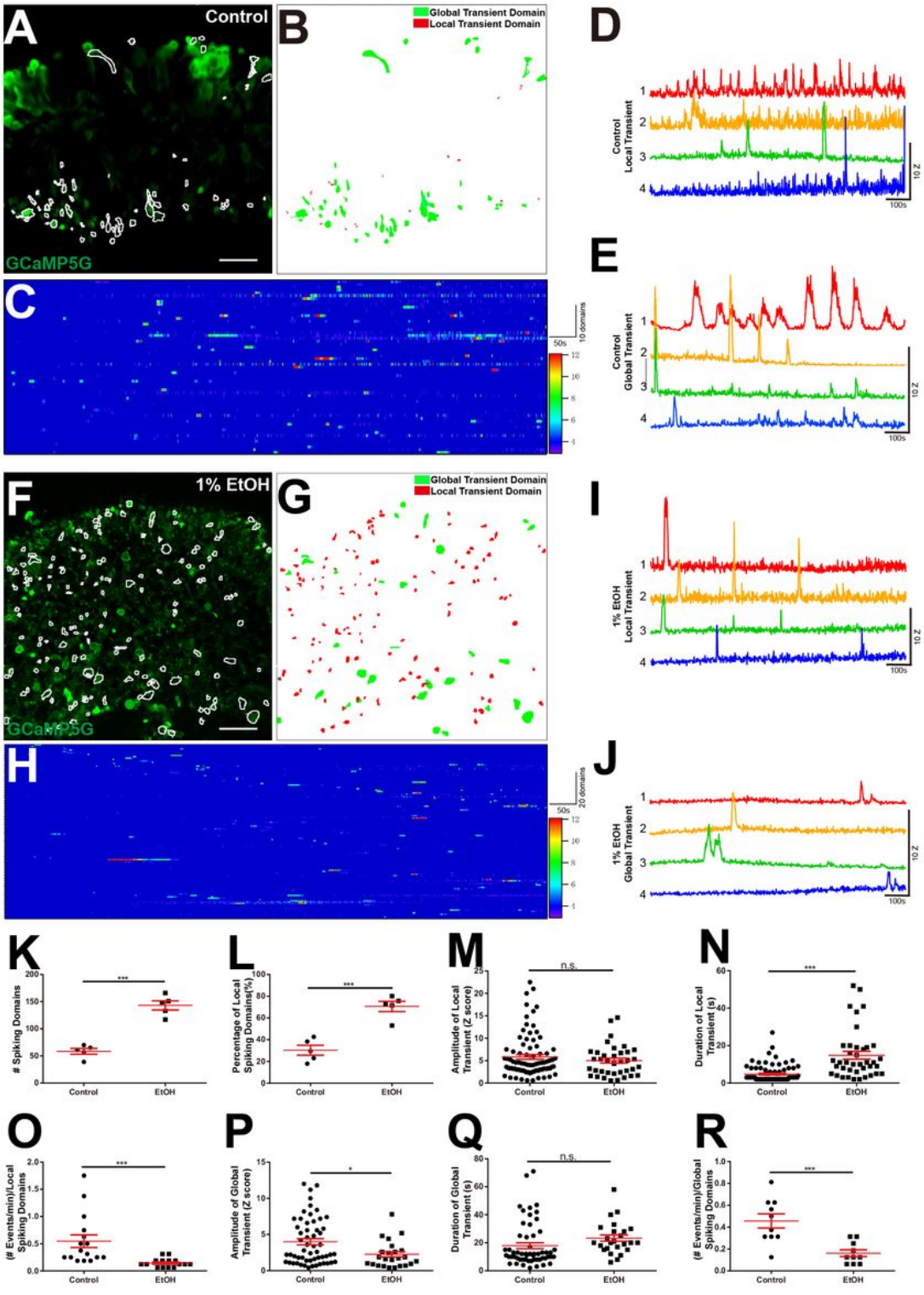

Figure 6

The calcium signaling dynamic was significantly altered in ethanol-treated hROs. **A** Median intensity projection image of 1000 frames from neural retina of hROs-GCaMP5G in control group. Map of

spontaneously active calcium spiking regions overlaid on image. **B** Map of calcium spiking regions recorded in control hROs-GCaMP5G (Red, local transient domain; Green, global transient domain). **C** Raster plots displaying time and intensity of calcium transients in the control hROs-GCaMP5G. Intensity versus time traces for calcium spiking regions (corresponding to **B**), showing characteristics of Ca^{2+} transients of local (**D**) and global transient domains (**E**). **F** Median intensity projection image of 1000 frames from neural retina of hROs-GCaMP5G in ethanol-treated group. Map of spontaneously active calcium spiking regions overlaid on image. **G** Map of calcium spiking regions recorded in ethanol treated hROs-GCaMP5G (Red, local transient domain; Green, global transient domain). **H** Raster plots displaying time and intensity of calcium transients in ethanol-treated hROs-GCaMP5G. Intensity versus time traces for calcium spiking regions (corresponding to **G**), showing characteristics of Ca^{2+} transients of local (**I**) and global transient domains (**J**). Graph of numbers of calcium spiking regions (**K**) and percentage of local transient domains (**L**) in hROs. M-O Graph showing amplitude per event (**M**), duration per event(**N**), and frequency of events per domain (**O**) in local transient domains of control and ethanol-treated hROs. Graph showing amplitude per event (**P**), duration per event(**Q**), and frequency of events per domain (**R**) in global transient domains of control and ethanol-treated hROs. Data are shown as mean ± SEM (n=3 independent experiments). *p < 0.05; **p < 0.01; ***p < 0.005. Scale bars: 25 μm for **A,F.**

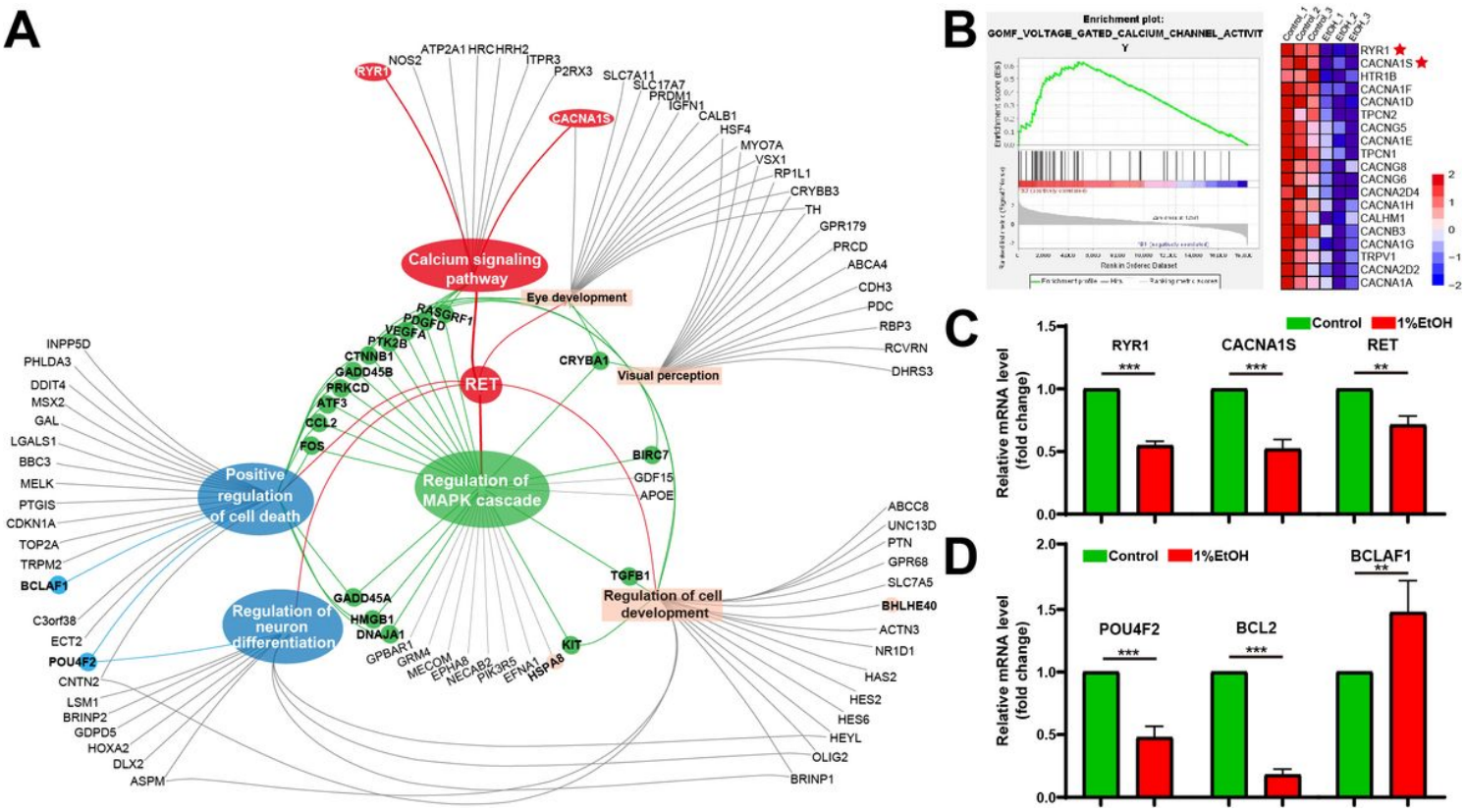

Figure 7

The enrichment of RYR1/CACNA1S/RET-dependent calcium signaling pathway to uncover the cell death and neuronal differentiation defect in ethanol-treated hROs. **A** Cnet plotting showing the interaction of 7 enriched pathways and genes associated with ethanol induced ocular aberration. Red line and circle

represent the main pathway enriched in Cnet plotting. Green line and circle represent the downstream pathways and genes. Blue line and circle represent target biological processes and possible target genes. **B** GSEA analysis for the voltage gated calcium channel activity between the control and ethanol treated hROs. **C~F** The qRT-PCR of target DEGs in D30 hROs of control and ethanol treated hROs. Data are mean ± SEM. n=3, three independent experiments. *p < 0.05; **p < 0.01; ***p < 0.005.

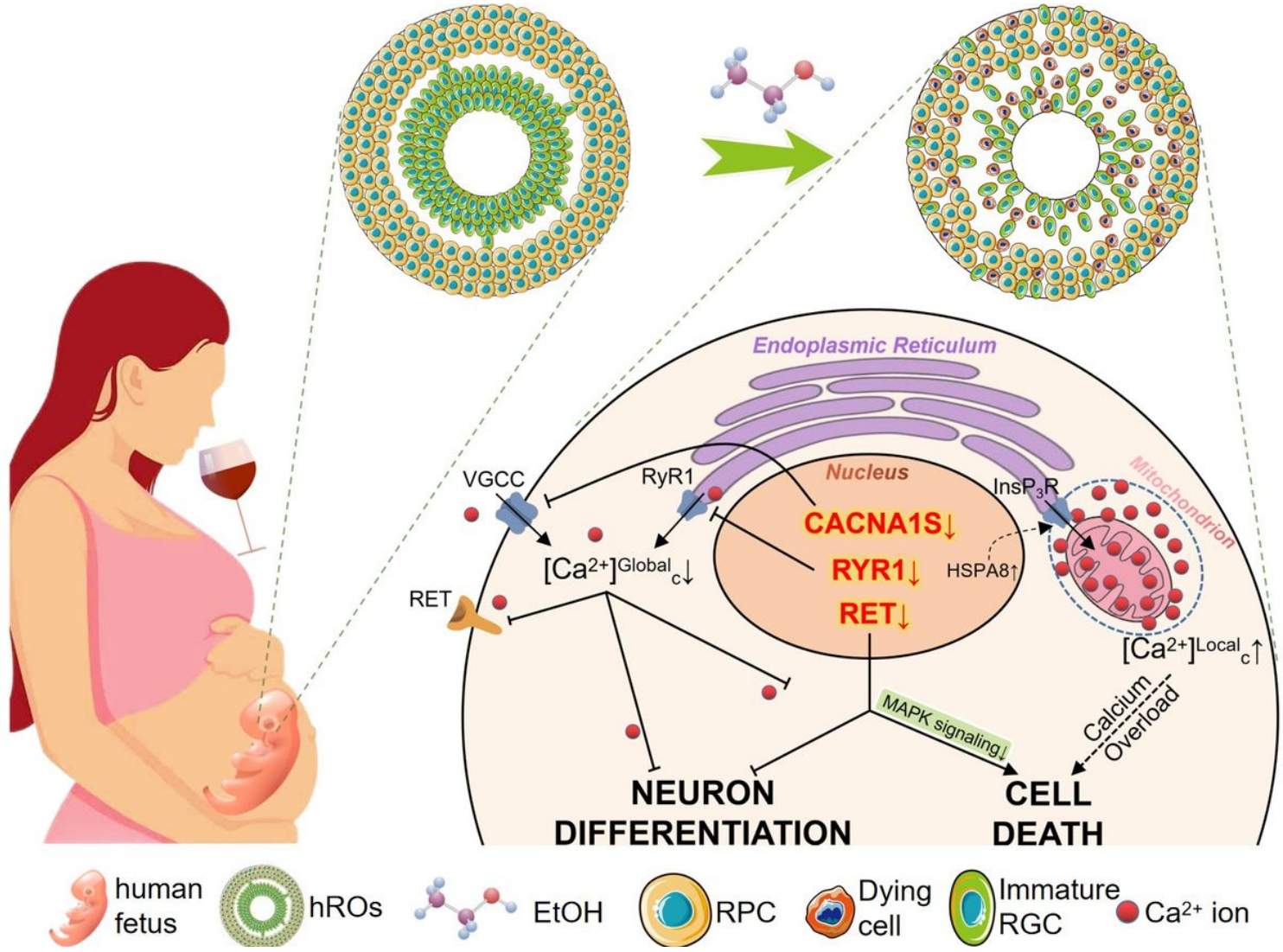

Figure 8

Schematic illustrates altered calcium signaling pathway in the ethanol-induced cell death and neuronal differentiation defect in hROs. Ethanol exposure impairs the retinal ganglion cell differentiation and induce robust cell death in hROs via calcium signaling pathway. Calcium channel RYR1 and CACNA1S containing voltage gated calcium channel both contribute to the cytosolic calcium dynamic perturbation after ethanol exposure. The decrease of global calcium transient pulls the brake on the neuronal differentiation while the enhancement of local calcium transient exacerbates the mitochondrial calcium overload which triggers the cell death. Moreover, the calcium binding protein RET act as a synergistical downstream effector to directly regulate the neuronal differentiation of retinal ganglion cells in hROs and indirectly contribute to cell death via MAPK signaling pathway.

Supplementary Files

This is a list of supplementary files associated with this preprint. Click to download.

- Additionalfle1Fig.S1..jpg
- Additionalfle2Fig.S2..jpg
- Additionalfle3Video1hESCsGCaMP5Gimaging.mp4
- Additionalfle3Video2hROsGCaMP5Gcontrolimaging.avi
- Additionalfle3Video3hROsGCaMP5GEtOHimaging.avi